ADVANCED MATERIALS
www.advmat.de

A Stretchable Graphitic Carbon/Si Anode Enabled by Conformal Coating of a Self-Healing Elastic Polymer

Yongming Sun, Jeffrey Lopez, Hyun-Wook Lee, Nian Liu, Guangyuan Zheng, Chun-Lan Wu, Jie Sun, Wei Liu, Jong Won Chung, Zhenan Bao, and Yi Cui**

Stretchable electronics have recently received intense attention due to their wide applications in various areas where devices must maintain intimate contact with curvilinear interfaces or undergo large deformation.[1] Lithium-ion batteries are the dominant power source for portable electronics and represent one of the most promising energy-storage systems for these stretchable electronic devices.[2] Two of the main challenges impeding the development of stretchable lithium-ion battery systems, however, are the limited stretchability and low specific energy. Recently, much effort has been devoted toward realizing the stretchability of battery systems. Several strategies have previously been successfully developed to achieve stretchable battery systems at the device level with stiff battery islands and stretchable interconnects (e.g., origami batteries[3] and serpentine interconnects[4]) and at the battery level through the use of buckled active materials on a prestrained substrate.[5] For the systems with device-level stretchability, the stability under stretching is still limited due to the rigidity of batteries. Worse still, the energy density of the overall battery systems is significantly reduced due to the large spacing between the small isolated battery islands. To achieve higher energy densities, the development of intrinsically stretchable electrodes is of key importance. Therefore, there is still an urgent need to explore electrodes with appreciable mechanical durability under strain for use in stretchable lithium-ion batteries.

Currently, $Li_4Ti_5O_{12}$ is the most widely used anode material for stretchable lithium-ion batteries due to its stable electrochemical properties.[5,6] However, it suffers from a low theoretical specific capacity (175 mAh g^{-1}) and high working potential (≈1.5 V), which greatly restrict the battery energy density. From this perspective, developing high-capacity anode materials with low working potentials is vital to achieve high specific energy in stretchable lithium-ion batteries. Little emphasis has been thus far placed on the development of high-capacity electrode materials for stretchable lithium-ion batteries, although success in this regard would allow much higher energy density for batteries. Among the anode materials, Si can deliver 24× theoretical capacity (4200 mAh g^{-1}) over $Li_4Ti_5O_{12}$ and has a much lower working potential (<0.5 V) compared with that of $Li_4Ti_5O_{12}$ (≈1.5 V).[7] Thus, it is highly desirable to explore Si anodes for stretchable lithium-ion batteries. Nevertheless, Si anodes have the serious issues of mechanical degradation and unstable solid-electrolyte interphase (SEI) due to the large volume expansion upon lithiation, which causes dramatic decay in battery performance.[8] Many attempts have been made to improve the electrochemical performance of Si anodes.[9] One of the most successful approaches has been the use of a self-healing polymer binder.[10] This soft and highly stretchable supramolecular polymer contains a large number of hydrogen bonding sites that allow it to mechanically heal at room temperature. The hydrogen bonding also helps the polymer adhere to the Si surface. This, combined with the self-healing ability, allows the formation of a stable SEI on Si during the large volumetric changes upon the lithiation and de-lithiation processes. This self-healing polymer is highly stretchable compared to traditional binder materials and has great potential to help realize stretchable Si electrodes via rational molecular design.

Normally, inorganic active electrode materials are stiff and rigid. The main approach to achieve stretchable electrodes is to create a stretchable structure out of normally non-stretchable active materials. Although a few of successful examples, such as buckled $Li_4Ti_5O_{12}$/carbon nanotube films on prestrained polydimethylsiloxane (PDMS) substrate[5a] and a spring-like carbon nanotube fibers,[5b] have been reported, there are still no reported high-capacity stretchable electrodes. Herein, for the first time, we demonstrate a high-capacity stretchable graphitic carbon/Si foam electrode enabled by conformal coating of a newly synthesized self-healing elastic polymer. Unlike the supramolecular self-healing polymer that was previously reported,[10] this material is much tougher due to a combination covalent crosslinks and sacrificial hydrogen bonds[11] and behaves elastically over a large range of strains. The amorphous Si layer on the graphitic carbon foam affords a high specific capacity, enabling a high overall capacity of 719 mAh g^{-1} for the graphitic carbon/Si composite electrode, four times that of the widely used $Li_4Ti_5O_{12}$ anode material for stretchable lithium-ion batteries, and maintained 81% of its

Dr. Y. M. Sun, Dr. H.-W. Lee, Dr. N. Liu, Dr. G. Y. Zheng, C.-L. Wu, Dr. J. Sun, Dr. W. Liu, Prof. Y. Cui
Department of Materials Science and Engineering
Stanford University
Stanford, CA 94305, USA
E-mail: yicui@stanford.edu
J. Lopez, Dr. J. W. Chung, Prof. Z. Bao
Department of Chemical Engineering
Stanford University
Stanford, CA 94305, USA
E-mail: zbao@stanford.edu
Dr. J. W. Chung
Samsung Advanced Institute of Technology
Yeongtong-gu, Suwon-si, Gyeonggi-do 443-803, South Korea
Prof. Y. Cui
Stanford Institute for Materials and Energy Sciences
SLAC National Accelerator Laboratory
Menlo Park, CA 94025, USA

DOI: 10.1002/adma.201504723

capacity after 100 cycles. Our investigations indicate that the self-healing elastomer is uniformly coated on the 3D graphitic carbon/Si foam and endows the composite electrode with high stretchability (up to 88%) and endures 1000 stretching-releasing cycles at 25% strain without detrimental resistance increases.

The stretchability of the electrode is realized via the deformation of the foam structure with the help from the self-healing elastomeric coating. As illustrated in **Figure 1**a, the composite electrode deforms and recovers the foam structure along the direction of mechanical strain. Previously, graphene/graphite foams were used as the current collectors to realize (flexible) high-rate $LiFePO_4$ and $Li_4Ti_5O_{12}$ electrodes[12] or high-capacity Si-based electrodes[13] due to their high conductivity. In the as-designed electrodes, the 3D graphitic carbon foam not only functions effectively as a current collector and provides high conductivity for electron transport, but also works as part of the active material alongside the amorphous Si on the surface of the carbon, which enables fast reaction dynamics in the initial charge/discharge progresses in comparison with crystalline Si. The highly elastic self-healing polymer helps to build a robust interface that improves the electrochemical stability of the electrode and maintains the active carbon/Si foam electrode integrity during the stretching and releasing processes, rendering the whole structure stretchable.

Figure 1b illustrates the preparation and optical microscope images of the stretchable graphitic carbon/Si/polymer composite electrode. The nickel foams have a 3D skeleton structure, and a graphitic carbon layer was first grown on the nickel through a chemical vapor deposition (CVD) process. Different from the previous work on the growth of thin graphene,[14] we obtained a mechanically robust thick graphitic carbon foam with a 3D hollow skeleton structure using a different carbon source (vaporized hexane) at ambient pressure. After the removal of nickel, an amorphous Si layer was conformably grown on the surface of 3D carbon foams using silane as the precursor under a low-pressure condition. Due to the hollow carbon skeleton and porous 3D structure, the deposition of Si is uniform throughout the entire carbon framework. A graphitic carbon/Si/polymer foam electrode was achieved after drop-coating a layer of self-healing polymer on the foam. Figure 1c shows a schematic for the synthesis of the self-healing elastomer modified from previously reported structures.[10,15] A mixture of fatty acid dimers and trimers (30:70) was reacted with excess diethylene triamine (DETA) to yield amine-terminated oligomers. Instead of reacting with urea to give a

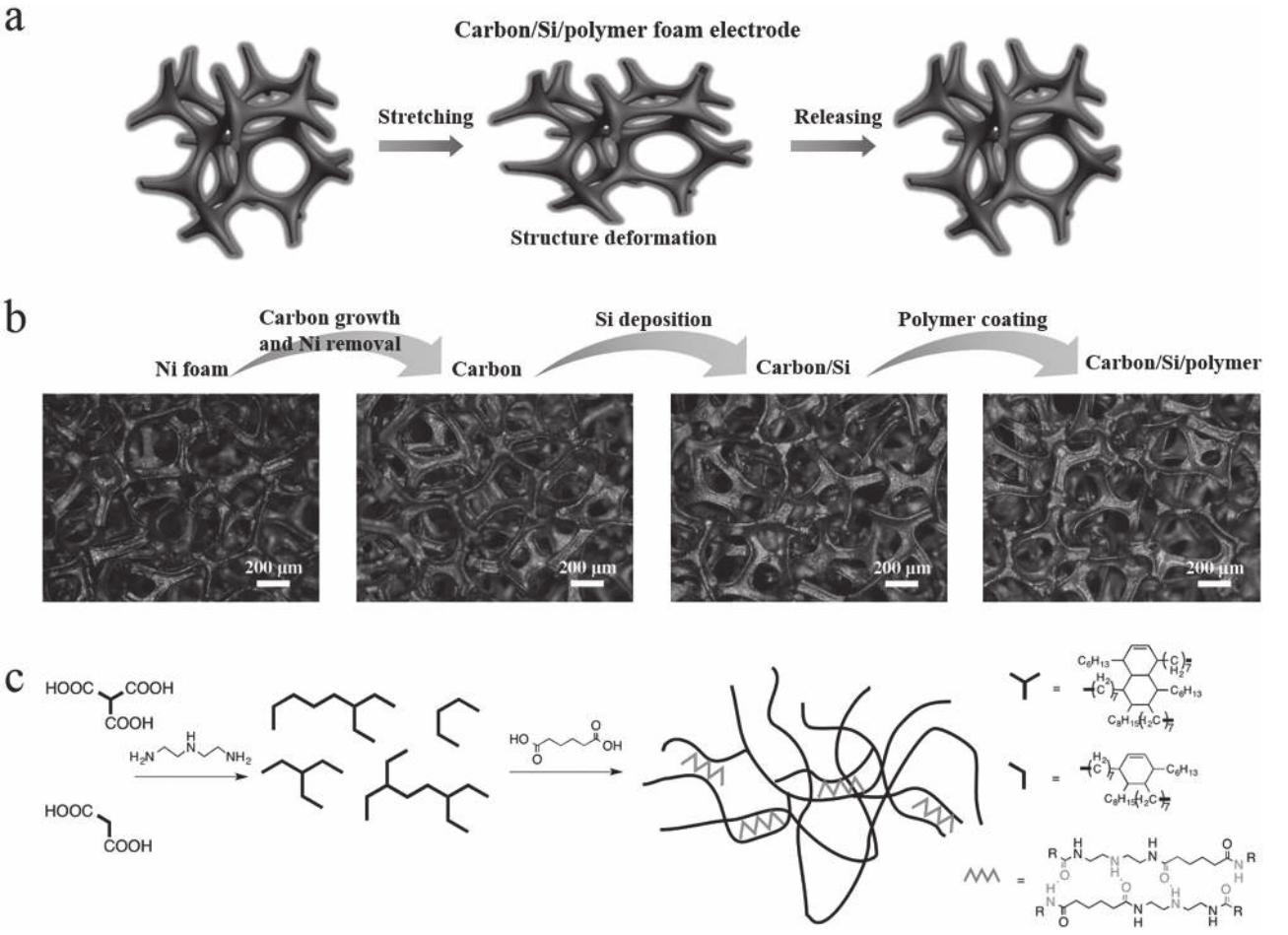

Figure 1. a) Schematic illustration of a stretching and releasing process for a carbon/Si/self-healing polymer foam electrode. b) Synthesis and optical microscope images of a carbon/Si/polymer foam electrode. c) Synthesis of the self-healing elastic polymer.

Adv. Mater. **2016**,
DOI: 10.1002/adma.201504723

viscoelastic supramolecular polymer as in previous reports, oligomers were further polymerized and cross-linked with adipic acid to produce the final elastomeric network with strong interchain hydrogen bonding interactions through the amide groups formed. Before coating, the amine oligomers and adipic acid were dissolved in ethanol (1 g/10 mL). The thickness of self-healing polymer coating could be controlled by adjusting the amount of solution used. The successful preparation of such conformal graphitic carbon/Si/polymer structure provides a great opportunity to achieve a high-capacity anode for stretchable lithium-ion batteries.

The investigation on the structure and crystallinity of the carbon/Si foam is critical for understanding its electrochemical and mechanical properties. **Figure 2**a shows the X-ray diffraction (XRD) patterns of the as-obtained carbon and carbon/Si foams. A sharp diffraction peak around 26.4° is observed for the carbon foam, which is readily ascribed to graphite (JCPDS No. 41–1487). No new peaks are observed for the carbon/Si foam, indicating the amorphous nature of the CVD-grown Si. The crystalline nature of carbon and amorphous structure of Si in the carbon/Si foam are further confirmed using Raman spectroscopy (Figure 2b,c). The so-called G band (≈1582 cm^{-1}), D band (≈1335 cm^{-1}), D′ band (≈1619 cm^{-1}), and G′ band (≈2674 cm^{-1}) are observed in the Raman spectrum, which are the most prominent features of graphite (Figure 2b).[16] Usually, crystalized Si is located at ≈520 cm^{-1} in the Raman spectrum. The existence of a broad peak at ≈475 cm^{-1} indicates the amorphous Si structure (Figure 2c).[17] The digital images show that the grey carbon foam turns blue after the CVD deposition of Si layer (Inset of Figure 2d and Figure S4, Supporting Information). It is observed under scanning electronic microscope (SEM) that the foam structures of carbon and carbon/Si hybrid are well maintained (Figure 2d and Figure S5, Supporting Information), consistent with observation under an optical microscope (Figure 1b). Due to the conformal growth of carbon on the nickel foam, the carbon and carbon/Si skeletons possess a hollow structure after the removal of the nickel skeleton, which is confirmed by a fractured carbon/Si skeleton (Figure 2e). Clearly, the smooth surface of the foam becomes rough after the CVD deposition of an amorphous Si layer (Figure 2f). Furthermore, transmission electron microscopy (TEM) investigation reveals that the Si layer on the surface of carbon is uniform throughout the observed area (Figure 2g). The electron energy loss spectroscopy (EELS) spectra recorded for the area in Figure 2g are shown in Figure 2h,i. Figure 2h shows the Si L2,3-edges, confirming the amorphous Si structure.[18] The EELS spectrum with the carbon K-edge shows well-defined peaks due to transitions of 1s electrons to π^* and σ^* antibonding states, indicating the graphitic nature of the carbon in the composite (Figure 2i).[19]

The mechanical properties of the self-healing polymer alone were investigated to understand its effects on the carbon/Si foam. After crosslinking, the self-healing polymer is highly elastic and can be stretched for about 400% before breaking. The toughness and strength of the material can be changed by controlling the crosslinking time (**Figure 3**a). 105 min is found to be the optimal crosslinking time because it gives a material with the highest modulus. In Figure S6 of the Supporting

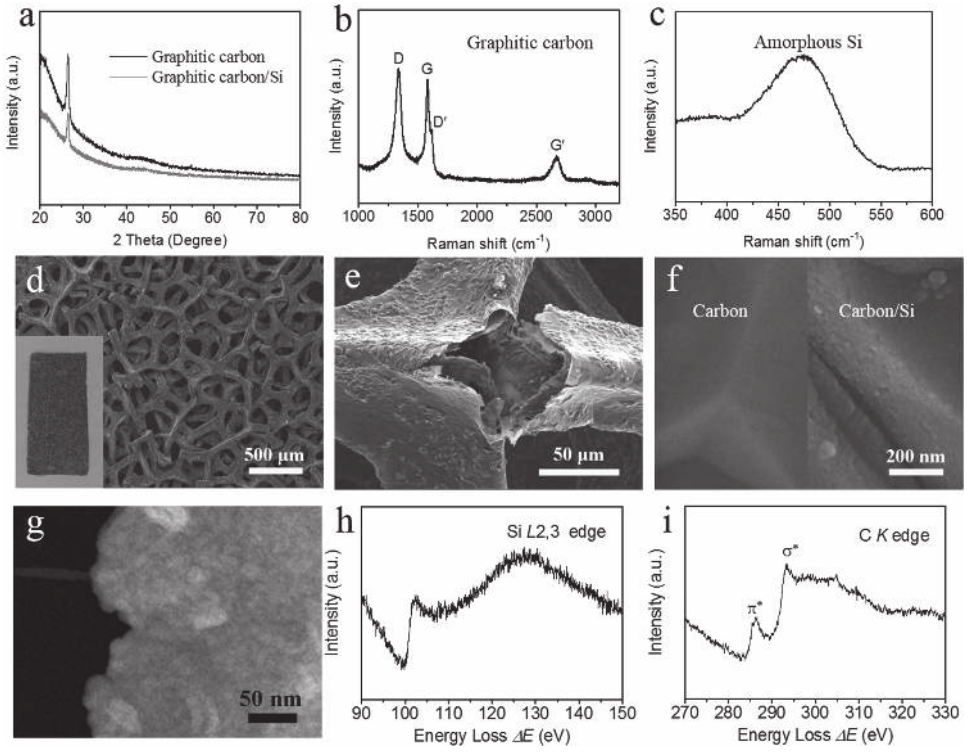

Figure 2. a) XRD patterns of the as-achieved carbon and carbon/Si foams. b,c) Raman spectra of the carbon/Si foam. d,e) SEM images of d) a carbon/Si foam and e) a fractured skeleton showing a hollow structure. f) High-magnification SEM images of the (left) carbon and (right) carbon/Si foams. g) TEM image of the carbon/Si foam. h,i) EELS spectra recorded for the area in g). The inset in d) shows a digital image of a carbon/Si foam.

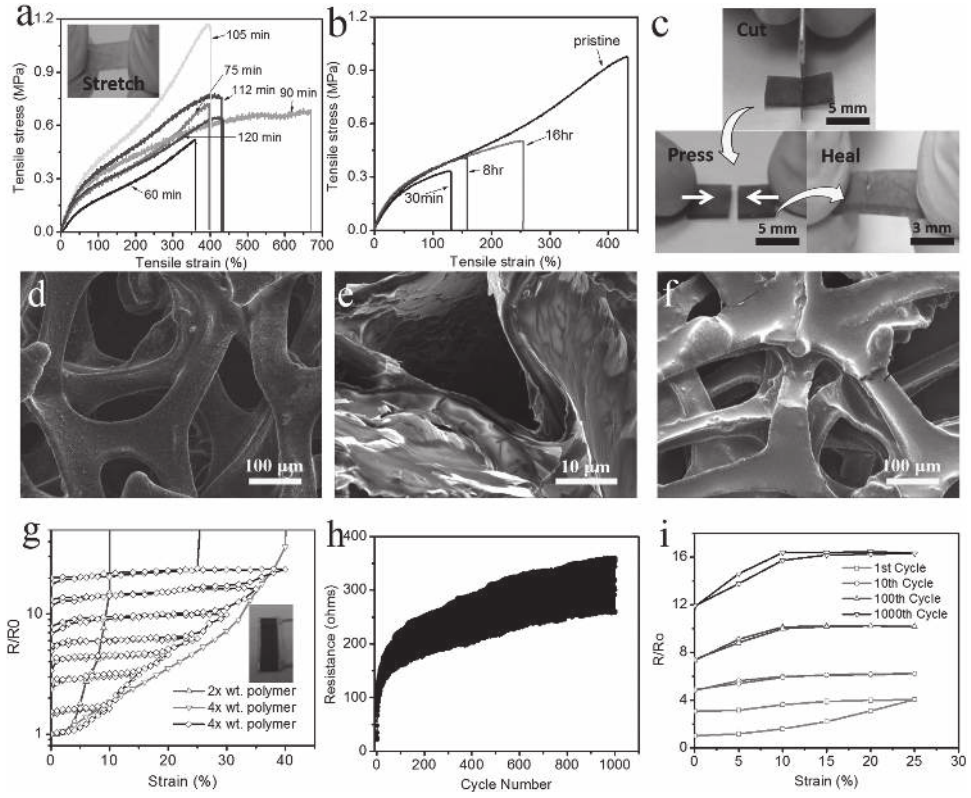

Figure 3. a) Stress–Strain curves for the bulk elastomer at different crosslinking reaction times. 105 min is found to be the optimal crosslinking time because it gives the material with the highest toughness. b) Self-healing of the bulk elastomer. Cut samples are allowed to rest for the prescribed time at room temperature and then compared to the performance of a pristine sample. c) Pictures of how the self-healing experiment is conducted. A sample is cut, pressed back together and then finally stretched until failure. d,e) SEM images of carbon/Si foams with 4× weight elastic polymer. f) SEM images of the carbon/Si foam electrodes with 4× weight elastic polymer after a ≈30% stretching-releasing cycle. g) Resistance vs strain curves of polymer coated carbon/Si foams supported on PDMS. Once stretched, resistance is stable at the final value until the foam is stretched further. h) Resistance measurements during strain cycling to 25%. Resistance increases over time. i) Highlighted cycles from h) show that resistance is relatively constant for any one cycle.

Information, the hysteresis of the bulk elastomer is shown. Strain cycles are applied consecutively, increasing by 100% each time. Very little hysteresis is observed up to 100% strain. Beyond that, more significant energy dissipation is seen and the material is not as tough upon re-stretching as in its pristine state. This energy dissipation comes from the sacrificial hydrogen bonds in the material, which break preferentially to the covalent crosslinks giving a much tougher elastomer.[11] The high density of hydrogen bonding sites also gives the elastomer a partial self-healing capability (Figure 3b). To test the self-healing, samples are cut into two pieces with a razor blade and then placed gently back together and allowed to rest at room temperature for the prescribed time (Figure 3c). Even after 30 min of healing at room temperature the modulus of the material is recovered and the healed sample can reach strains past 100%. Further healing was achieved up to 16 h, after which no further healing was observed. This incomplete healing is due to the irrecoverable fracture of the covalent crosslinks in the network. The hydrogen bonding sites are only capable of restoring a portion of the materials original mechanical properties. This bulk self-healing experiment is an extreme test of the healing ability of the material. In a device that is stretching to 50%, local strains large enough to fully fracture the elastomer will be rare and so the healing will instead act to restore the elasticity and strength of the material as it is strained and released. The self-healing elastic polymer possesses plenty of hydrogen-bonding sites to interact with the Si—OH on the Si surface (Figure 1c) and thus provides good adhesion to the Si layers.[10a] This is evidenced by the C=O stretching and the NH bending peaks in the Fourier transform infrared (FTIR) spectrum (Figure S7, Supporting Information), at ≈1650 cm^{-1} and ≈3250 cm^{-1}, respectively, that correspond to disordered hydrogen bonding of the amide groups, and a lack of a peak or shoulder near 1690 cm^{-1} that corresponds to "free" carbonyl groups.[20] The hydrogen bonding interaction with Si—OH on the Si surface has been observed in many other binders including CMC, alginate, and cyclodextrin.[21] The intimate contact between the elastic polymer layer and the surface of carbon/Si foam is confirmed by the SEM images (Figure 3d,e, and Figure S8, Supporting Information). Once the electrode undergoes strain, the self-healing elastic polymer can help to keep the foam structure intact.

Next, we quantified the stretchability dependence of the carbon/Si/polymer composite electrode on the amounts of the elastic polymer. Figure S9 of the Supporting Information shows stress–strain curves for the elastic polymer coated carbon/Si

Adv. Mater. 2016,
DOI: 10.1002/adma.201504723

foams. As the amount of the elastic polymer increases, the foam gains increased stretchability because the connectivity of the polymeric network on the foam increases with thickness of the polymer layer. With 2× weight polymer the coating is thin and large cracks can be seen after 30% strain for the composite foam on a PDMS substrate (Figure S10a, Supporting Information). As the coating amount is increased to 4× weight and then 6× weight, the cracks get smaller and for the 6× weight polymer sample, polymer can be seen bridging different parts of the carbon/Si foam before and after cracking (Figure 3f and Figure S10b, Supporting Information). This increasingly connected polymer network allows for better stress dissipation through the sacrificial hydrogen bonds of the elastomer, and if polymer loading were to be further increased, the mechanical properties of the composite foam would eventually become similar to those of the bulk elastomer.

Over this stretching and releasing processes the electronic conductivity of the electrodes may change, which influences the battery performance. Elastic polymer films, such as PDMS, are widely used as the electrode substrates and packages for flexible and stretchable lithium-ion batteries.[4,5a,12a,22] In order to study the electronic conductivity of the composite foams and mimic the structure of a fully assembled stretchable battery under strain, the composite foams were loaded on an elastic PDMS substrate and strained. As the supported composite foams were stretched, small cracks formed across the length and width of the material to dissipate the stress and allowed the foams to maintain their electronic conductivity to strains far past values at which the unsupported foams would completely fail. For the 4× weight polymer composite foams, the average failure strain was 46.2% (±22.9%) and the best performing electrode reached a strain of 88% before it was no longer conductive (Figure 3g). This is also a significant improvement compared to our previously reported supramolecular self-healing polymer,[10] which only enabled an average strain of 8.5% (±3.5%) before electrode failure at the same wt% (Figure S11, Supporting Information). As the electrode was initially stretched, the resistance increased due to the new cracks that formed, but upon releasing the resistance was maintained at a constant value. The resistance stayed at this value until an even larger strain was applied, when the resistance again increased corresponding to the new strain that was applied. As further strain was applied, the hysteresis curve overlapped with that of a pristine electrode being strained for the first time. This again shows that an increase in resistance only occurs for strains past that already experienced by the electrode. Using these electrodes, it should be possible to achieve strains of 30%–50% in a full-cell stretchable device.

Since a stretchable lithium-ion battery has to undergo repeated stretching-releasing cycles over its lifespan, it is important to understand the stability of these electrodes during strain cycling. The electrodes were subjected to 1000 cycles of loading and unloading at a strain of 25% (Figure 3h). Confined by the elastic outer self-healing polymer layer, the overall electrode structure was kept intact. Over the many cycles, the resistance did drift upward to some extent but it did not reach values that are unacceptable for use as a battery electrode (<400 Ω after 1000 cycles). While drift was observed over many cycles, any one cycle from this data set did not show any large resistance increases (Figure 3i). If the cycling experiment is extended further, it is likely that the resistance would reach a plateau value as the system found an equilibrium state.

With the optimized amount of self-healing elastic polymer, the carbon/Si foam electrode affords remarkable battery performance. **Figure 4**a shows the reversible delithiation specific capacities of the carbon/Si electrodes coated with different amounts of self-healing polymer over 100 charge/discharge cycles. Here, all reported capacities are calculated based on the total weight of carbon and Si unless otherwise mentioned. The initial specific delithiation capacity of the pristine carbon/Si electrode reaches 1064 mAh g^{-1}, while the value for the bare carbon foam is 197 mAh g^{-1}. Considering that the Si amount in the carbon/Si electrode is ≈30%, the specific capacity with respect to Si is calculated to be as high as 3087 mAh g^{-1}. After coated with 2× and 4× weight self-healing elastic polymer, the carbon/Si electrodes deliver their initial delithiation capacities of 872 and 719 mAh g^{-1}, respectively. With a thicker self-healing polymer coating layer (6× weight polymer), the carbon/Si electrode only delivers 49% specific capacity (517 mAh g^{-1}) of the value that the pristine carbon/Si electrode achieves. Due to a relatively low ionic conductivity of 2.68×10^{-4} S/cm ($\pm 0.88 \times 10^{-4}$) in the dry state and 4.24×10^{-4} S cm^{-1} ($\pm 1.56 \times 10^{-4}$) in the swollen state (Figure S12, Supporting Information), a thick self-healing polymer coating layer may lead to increased lithium-ion diffusion paths, large electrode series resistance, and thus a relatively low capacity when compared with electrodes coated with a thinner polymer film. PDMS is the most widely used elastic matrix for stretchable devices. Here, we also tested PDMS as a potential elastic support for the carbon/Si foam, and while the PDMS formed a good coating on the foam (Figure S13, Supporting Information), the electrochemical performance was very poor due to the poor Li conductivity (Figure S14, Supporting Information). This shows that both the mechanical and chemical properties are important when selecting an elastomer support.

Besides the difference in the reversible specific capacities, as shown in Figure 4a, the electrodes coated with various amounts of self-healing polymer exhibit different cycle stability. The specific capacity of the pristine carbon/Si electrode after 100 charge/discharge cycles is 491 mAh g^{-1} with a low capacity retention of 46%. Coated with proper amounts of self-healing polymer, the electrodes possess much improved cycling stability. With 2× weight polymer, the carbon/Si electrode achieves a high specific capacity of 722 mAh g^{-1} after 100 charge/discharge cycles. The corresponding capacity retention is as high as 83% with 0.17% decay per cycle. When the amount of self-healing polymer increases to 4× weight polymer, the reverse specific capacity of the electrode is 584 mAh g^{-1} at the 100th cycle, which is still more than three times the theoretical capacity of $Li_4Ti_5O_{12}$, showing a similar capacity retention (81%) to the electrode with 2× weight polymer. The investigations on the morphology of the carbon/Si/polymer electrode and the pristine carbon/Si electrode after cycling show that the SEI layer on the surface of the pristine carbon/Si electrode is much thicker than that of the polymer coated electrode (Figure S15, Supporting Information), which explains the enhanced cycling performance of the self-healing polymer coated carbon/Si electrodes. Moreover, the graphitic carbon/Si/self-healing polymer electrodes after strain cycling still exhibit stable cycling only with a little faster decay in

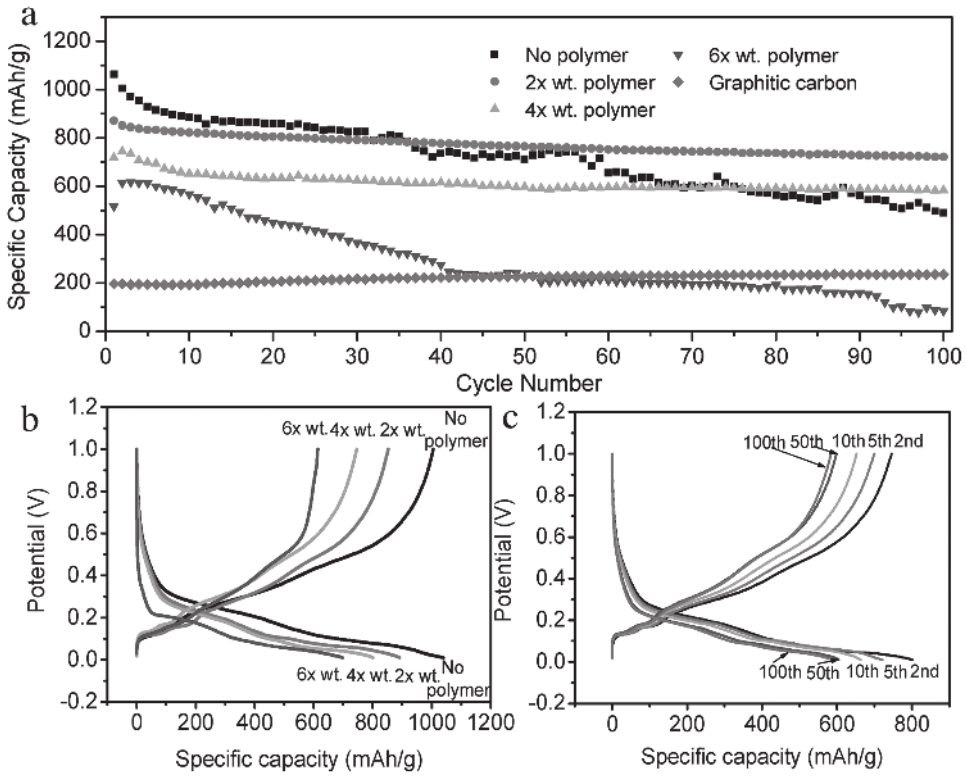

Figure 4. a) Specific delithiation capacities of the carbon/Si electrodes with different amounts of the self-healing polymer and the bare carbon electrode at the current density of 100 mA g^{-1} over cycling. b) Typical voltage profiles for the carbon/Si electrodes with different amounts of the self-healing polymer (second cycle). c) Voltage profiles of a carbon/Si electrode coated with 4× weight self-healing elastic polymer upon cycling.

capacity upon cycling, compared to the foam electrodes without undergoing strain cycling (Figure S16, Supporting Information). The much improved cycling performance is a strong indication of the structure enhancement and self-healing effect of the polymer helping keep the electrode intact. However, further increasing the amount of self-healing polymer (e.g., 6× weight polymer) leads to rapid capacity decay. The electrode almost loses all the capacity after 100 charge/discharge cycles (only 86 mAh g^{-1} for the 100th cycle). Regardless of their specific capacities, all the tested electrodes show stable Coulombic efficiency after the initial cycles (e.g., 99% from 12 to 100th cycle for the electrode with 4× weight polymer, Figure S17, Supporting Information). Therefore, to avoid low specific capacities and poor cyclability, a relative thin polymer coating layer is needed. Nevertheless, to obtain good stretchability, a relative thick polymer coating layer is preferred. In term of both electrochemical performances and stretchability, our results suggest that a 4× weight polymer amount is optimal and can meet the requirements of high capacities, stable cycling stability and good stretchability. Under the same electrochemical measurement condition, we also investigated the cyclability of the bare carbon foam electrode. The as-synthesized carbon electrode exhibits typical voltage profiles of graphite anodes with stable cycling (Figure 4a and Figure S18, Supporting Information).[23] It has been confirmed that the electric conductivity of graphite increases after the lithium insertion and can reach two orders of magnitude of the initial value.[24] Thus, the graphitic carbon skeleton of our electrodes can keep the entire electrode highly conductive during the charge/discharge cycles. The typical voltage profiles of the carbon/Si electrodes coated with different amount of self-healing polymer are shown in Figure 4b. With the increasing amount of the self-healing polymer, gradually decreased reversible specific capacities and slightly increased over potential are observed, arising from the low electronic conductivity and increased lithium-ion diffusion distance on the surface of the electrodes. Figure 4c shows the voltage profiles of a carbon/Si electrode coated with 4× weight polymer upon cycling. In spite of slight capacity decay, the charge/discharge curves remain steady and reversible even after 100 cycles.

In summary, stretchable lithium-ion batteries present unique opportunities for stretchable electronics but also limitations (e.g., low-energy density and limited stretchability). We have designed a conformal graphitic carbon/Si/self-healing elastic polymer foam structure to successfully achieve a high-capacity long-lifespan anode for stretchable lithium-ion batteries. Our demonstration here of a graphitic carbon/Si composite that has a high reversible specific capacity and a self-healing elastic polymer that enables long battery cycle life and good stretchability indicates a rational design for high-capacity stretchable electrodes. In comparison to the widely-used $Li_4Ti_5O_{12}$ anode material in stretchable lithium-ion batteries, the features of a high reversible specific capacity and low working potential are of key importance for the improvement of energy and power densities of the entire battery. This work presents an effective route in developing high-capacity Si-based anodes for stretchable lithium-ion batteries for the first time and paves the

Adv. Mater. **2016**,
DOI: 10.1002/adma.201504723

way for their promising applications in stretchable electronics. The successful stretchable structure design using a self-healing elastic polymer could also be extended to other stretchable material systems for various stretchable devices.

Supporting Information

Supporting Information is available from the Wiley Online Library or from the author.

Acknowledgements

Y.M.S. and J.L. contributed equally to this work. This work was supported by Samsung Electronics.

Received: September 25, 2015
Revised: November 21, 2015
Published online:

[1] a) S. Xu, Y. H. Zhang, L. Jia, K. E. Mathewson, K.-I. Jang, J. Kim, H. R. Fu, X. Huang, P. Chava, R. H. Wang, S. Bhole, L. Z. Wang, Y. J. Na, Y. Guan, M. Flavin, Z. S. Han, Y. G. Huang, J. A. Rogers, *Science* **2014**, *344*, 70; b) D.-H. Kim, N. S. Lu, R. Ma, Y.-S. Kim, R.-H. Kim, S. D. Wang, J. Wu, S. M. Won, H. Tao, A. Islam, K. J. Yu, T.-I. Kim, R. Chowdhury, M. Ying, L. Z. Xu, M. Li, H.-J. Chung, H. Keum, M. McCormick, P. Liu, Y.-W. Zhang, F. G. Omenetto, Y. G. Huang, T. Coleman, J. A. Rogers, *Science* **2011**, *333*, 838; c) D. Son, J. Lee, S. T. Qiao, R. Ghaffari, J. Kim, J. E. Lee, C. Song, S. J. Kim, D. J. Lee, S. W. Jun, S. X. Yang, M. Park, J. Shin, K. Do, M. Lee, K. Kang, C. S. Hwang, N. S. Lu, T. Hyeon, D.-H. Kim, *Nat. Nanotechnol.* **2014**, *9*, 397.

[2] a) N.-S. Choi, Z. H. Chen, S. A. Freunberger, X. L. Ji, Y.-K. Sun, K. Amine, G. Yushin, L. F. Nazar, J. Cho, P. G. Bruce, *Angew. Chem. Int. Ed.* **2012**, *51*, 9994; b) M. Armand, J.-M. Tarascon, *Nature* **2008**, *451*, 652; c) B. Scrosati, J. Hassoun, Y.-K. Sun, *Energy Environ. Sci.* **2011**, *4*, 3287.

[3] Z. M. Song, T. Ma, R. Tang, Q. Cheng, X. Wang, D. Krishnaraju, R. Panat, C. K. Chan, H. Y. Yu, H. Q. Jiang, *Nat. Commun.* **2014**, *5*, 3140.

[4] S. Xu, Y. H. Zhang, J. Cho, J. Lee, X. Huang, L. Jia, J. A. Fan, Y. W. Su, J. Su, H. G. Zhang, H. Y. Cheng, B. W. Lu, C. J. Yu, C. Chuang, T.-i. Kim, T. Song, K. Shigeta, S. Kang, C. Dagdeviren, I. Petrov, U. Paik, J. A. Rogers, *Nat. Commun.* **2013**, *4*, 1543.

[5] a) W. Weng, Q. Sun, Y. Zhang, S. S. He, Q. Q. Wu, J. Deng, X. Fang, G. Z. Guan, J. Ren, H. S. Peng, *Adv. Mater.* **2015**, *27*, 1363; b) Y. Zhang, W. Y. Bai, X. L. Cheng, J. Ren, W. Weng, P. N. Chen, X. Fang, Z. T. Zhang, H. S. Peng, *Angew. Chem. Int. Ed.* **2014**, *53*, 14564.

[6] Y. Liu, S. Gorgutsa, C. Santato, M. Skorobogatiy, *J. Electrochem. Soc.* **2012**, *159*, A349.

[7] C. K. Chan, H. L. Peng, G. Liu, K. McIlwrath, X. F. Zhang, R. A. Huggins, Y. Cui, *Nat. Nanotechnol.* **2008**, *3*, 31.

[8] H. Wu, Y. Cui, *Nano Today* **2012**, *7*, 414.

[9] a) N. Liu, Z. D. Lu, J. Zhao, M. T. McDowell, H.-W. Lee, W. T. Zhao, Y. Cui, *Nat. Nano* **2014**, *9*, 187; b) N. Liu, H. Wu, M. T. McDowell, Y. Yao, C. M. Wang, Y. Cui, *Nano Lett.* **2012**, *12*, 3315; c) H. Wu, G. Chan, J. W. Choi, I. Ryu, Y. Yao, M. T. McDowell, S. W. Lee, A. Jackson, Y. Yang, L. B. Hu, Y. Cui, *Nat. Nanotechnol.* **2012**, *7*, 310; d) H. Wu, G. H. Yu, L. J. Pan, N. Liu, M. T. McDowell, Z. N. Bao, Y. Cui, *Nat. Commun.* **2013**, *4*, 1943; e) H. Kim, B. Han, J. Choo, J. Cho, *Angew. Chem.* **2008**, *120*, 10305; f) A. Magasinski, P. Dixon, B. Hertzberg, A. Kvit, J. Ayala, G. Yushin, *Nat. Mater.* **2010**, *9*, 353.

[10] a) C. Wang, H. Wu, Z. Chen, M. T. McDowell, Y. Cui, Z. N. Bao, *Nat. Chem.* **2013**, *5*, 1042; b) Z. Chen, C. Wang, J. Lopez, Z. D. Lu, Y. Cui, Z. N. Bao, *Adv. Energy Mater.* **2015**, *8*, 1401826.

[11] a) J.-Y. Sun, X. H. Zhao, W. R. K. Illeperuma, O. Chaudhuri, K. H. Oh, D. J. Mooney, J. J. Vlassak, Z. G. Suo, *Nature* **2012**, *489*, 133; b) E. Ducrot, Y. L. Chen, M. Bulters, R. P. Sijbesma, C. Creton, *Science* **2014**, *344*, 186.

[12] a) N. Li, Z. P. Chen, W. C. Ren, F. Li, H.-M. Cheng, *Proc. Natl. Acad. Sci. USA* **2012**, *109*, 17360. b) H. X. Ji, L. L. Zhang, M. T. Pettes, H. F. Li, S. S. Chen, L. Shi, R. Piner, R. S. Ruoff, *Nano Lett.* **2012**, *12*, 2446.

[13] J. Y. Ji, H. X. Ji, L. L. Zhang, X. Zhao, X. Bai, X. B. Fan, F. B. Zhang, R. S. Ruoff, *Adv. Mater.* **2013**, *25*, 4673.

[14] Z. P. Chen, W. C. Ren, L. B. Gao, B. L. Liu, S. F. Pei, H.-M. Cheng, *Nat. Mater.* **2011**, *10*, 424.

[15] P. Cordier, F. Tournilhac, C. Soulié-Ziakovic, L. Leibler, *Nature* **2008**, *451*, 977.

[16] M. A. Pimenta, G. Dresselhaus, M. S. Dresselhaus, L. G. Cancado, A. Jorio, R. Saito, *Phys. Chem. Chem. Phys.* **2007**, *9*, 1276.

[17] S. M. Kang, K. M. Ahn, B. T. Ahn, *J. Electrochem. Soc.* **2012**, *159*, H29.

[18] M. Schade, N. Geyer, B. Fuhrmann, F. Heyroth, H. S. Leipner, *Appl. Phys. A* **2009**, *95*, 325.

[19] A. A. El-Barbary, S. Trasobares, C. P. Ewels, O. Stephan, A. V. Okotrub, L. G. Bulusheva, C. J. Fall, M. I. Heggie, *J. Phys.: Conf. Ser.* **2006**, *26*, 149.

[20] M. M. Coleman, M. Sobkowiak, G. J. Pehlert, P. C. Painter, T. Iqbal, *Macromol. Chem. Phys.* **1997**, *198*, 117.

[21] a) J. S. Bridel, T. Azaïs, M. Morcrette, J.-M. Tarascon, D. Larcher, *Chem. Mater.* **2010**, *22*, 1229; b) I. Kovalenko, B. Zdyrko, A. Magasinski, B. Hertzberg, Z. Milicev, R. Burtovyy, I. Luzinov, G. Yushin, *Science* **2011**, *334*, 75; c) Y. K. Jeong, T.-W. Kwon, I. Lee, T.-S. Kim, A. Coskun, J. W. Choi, *Nano Lett.* **2014**, *14*, 864.

[22] Q. Sun, X. Fang, W. Weng, J. Deng, P. N. Chen, J. Ren, G. Z. Guan, M. Wang, H. S. Peng, *Angew. Chem. Int. Ed.* **2015**, *127*, 10685.

[23] N. A. Kaskhedikar, J. Maier, *Adv. Mater.* **2009**, *21*, 2664.

[24] W. Bao, J. Y. Wan, X. G. Han, X. H. Cai, H. L. Zhu, D. Kim, D. Ma, Y. L. Xu, J. N. Munday, H. D. Drew, M. S. Fuhrer, L. B. Hu, *Nat. Commun.* **2014**, *5*, 4224.